Molecular Therapy
Nucleic Acids
Original Article

Hair cell-specific Myo15 promoter-mediated gene therapy rescues hearing in DFNB9 mouse model

Hui Wang,[1,2,3,4] MengZhao Xun,[1,2,3,4] Honghai Tang,[1,2,3,4] Jingjing Zhao,[1,2,3] Shaowei Hu,[1,2,3] Longlong Zhang,[1,2,3] Jun Lv,[1,2,3] Daqi Wang,[1,2,3] Yuxin Chen,[1,2,3] Jianping Liu,[1,2,3] Geng-lin Li,[1,2,3] Wuqing Wang,[1,2,3] Yilai Shu,[1,2,3] and Huawei Li[1,2,3]

[1]ENT Institute and Otorhinolaryngology Department of Eye & ENT Hospital, State Key Laboratory of Medical Neurobiology and MOE Frontiers Center for Brain Science, Fudan University, Shanghai 200031, China; [2]Institutes of Biomedical Science, Fudan University, Shanghai 200032, China; [3]NHC Key Laboratory of Hearing Medicine, Fudan University, Shanghai 200031, China

Adeno-associated viral (AAV) vectors are increasingly used as vehicles for gene delivery to treat hearing loss. However, lack of specificity of the transgene expression may lead to overexpression of the transgene in nontarget tissues. In this study, we evaluated the expression efficiency and specificity of transgene delivered by AAV-PHP.eB under the inner ear sensory cell-specific Myo15 promoter. Compared with the ubiquitous CAG promoter, the Myo15 promoter initiates efficient expression of the GFP fluorescence reporter in hair cells, while minimizing non-specific expression in other cell types of the inner ear and CNS. Furthermore, using the Myo15 promoter, we constructed an AAV-mediated therapeutic system with the coding sequence of *OTOF* gene. After inner ear injection, we observed apparent hearing recovery in *Otof* $^{-/-}$ mice, highly efficient expression of exogenous otoferlin, and significant improvement in the exocytosis function of inner hair cells. Overall, our results indicate that gene therapy mediated by the hair cell-specific Myo15 promoter has potential clinical application for the treatment of autosomal recessive deafness and yet for other hereditary hearing loss related to dysfunction of hair cells.

INTRODUCTION

Hearing loss is one of the most common sensory deficits in humans, with 466 million people affected worldwide.[1] Hereditary hearing loss accounts for more than 50% of childhood hearing loss.[2] The current therapeutic strategies in clinical practice focus mainly on hearing aids or cochlear implants. Although these methods have made great progress in alleviating deafness, the sound quality patients perceive cannot match that of the normal ear. Speech perception in noisy environments and music perception are also big hurdles for patients with cochlear implant.[3,4] Thus, it is urgent to explore novel therapeutic strategies. Recently, given the increased understanding of the mechanisms of hearing loss,[5–7] as well as the development of gene therapy in other systems, cochlear gene therapy has emerged as a promising strategy. More excitingly, gene therapy drugs for deafness caused by *OTOF* gene mutations are entering clinical trials. It will be a start for clinical trials of gene therapy for hearing loss; moreover, it can be predicted that more and more gene therapy drugs for deafness will be applied clinically in the future. Therefore, any possible measures that could enhance the specificity and safety of cochlear gene therapy are crucial.

Adeno-associated viral (AAV) vectors are extensively used as delivery vehicles in gene therapy because of their low pathogenicity, low immunogenicity, and stable expression.[8] In addition to the AAV capsid, the promoter is also a key factor for the expression distribution and level of the transgenes. Commonly used ubiquitous promoters, including the chicken beta-actin (CBA) promoter, the cytomegalovirus (CMV)-beta-globin promoter, and the CAG promoter (the CBA promoter with the CMV IE enhancer), are popular because they initiate potent expression of transgenes in multiple cell types. These ubiquitous promoters in cooperation with engineered AAV capsids could enable highly efficient transduction and transcription of therapeutic systems in the inner ear. However, overexpression of transgenes in nontarget tissues may lead to adverse effects, including degeneration of neurons, liver dysfunction, and coagulation disorders.[9,10] For this reason, ubiquitous promoters are not ideal regulatory elements for gene therapy. Instead, cell-type-specific promoters

Received 18 September 2023; accepted 30 January 2024;
https://doi.org/10.1016/j.omtn.2024.102135.

[4]These authors contributed equally

Correspondence: Wuqing Wang, State Key Laboratory of Medical Neurobiology and MOE Frontiers Center for Brain Science, Fudan University, Shanghai 200031, China.
E-mail: wwuqing@eent.shmu.edu.cn
Correspondence: Yilai Shu, State Key Laboratory of Medical Neurobiology and MOE Frontiers Center for Brain Science, Fudan University, Shanghai 200031, China.
E-mail: yilai_shu@fudan.edu.cn
Correspondence: Huawei Li, State Key Laboratory of Medical Neurobiology and MOE Frontiers Center for Brain Science, Fudan University, Shanghai 200031, China.
E-mail: hwli@shmu.edu.cn

would minimize the expression of transgenes in nontarget tissues and enable transgenes to more closely resemble physiological expression levels.

The cochlea is a sophisticated and compact organ that contains many distinct cell types, including hair cells (HCs), supporting cells, spiral ganglion neurons (SGNs), and stria vascularis cells; thus, mutual regulation among cell types is critical to the normal function of the cochlea.[11] Thus, the precise targeting of gene delivery is essential to the success of gene therapy. Cochlear HCs are the sensory cells of the auditory system and consist of two cell types. Outer HCs (OHCs) are responsible for amplifying and tuning sound signals, and inner HCs (IHCs) are responsible for converting mechanical impulses into electrical signals and transmitting these signals to SGNs.[12] Degeneration or loss of function of HCs is the most common cause of hereditary hearing loss,[13,14] as more than half of deafness genes are located in HCs,[15] such as *Otof*, *Atoh1*, *Myo15a*, *Myo7a*, *Pou4f3*, *Kcnq4*, and *Myo6*; thus HCs are one of the primary cell types of interest in the field of cochlear gene therapy.[16,17] To date, the promoters that drive specific expression to the HCs are very limited, and the initiation ability and the spatiotemporal specificity of these promoters limit their application.[18,19] The Myo7a promoter could drive transgene expression exclusively in HCs,[20] but Liu et al.[21] showed that the transcription level driven by the Myo7a promoter was lower than that of the ubiquitous CAG promoter, indicating that it is not suitable for the use of gene therapy. Therefore, the development of potent HC-specific promoter is essential for the clinical transformation of cochlea gene therapy. A previous study demonstrated that the Cre gene fused with the artificial Myo15 promoter sequence could specifically regulate gene expression in HCs.[22] Thus, we assumed that gene expression mediated by the Myo15 promoter might be a candidate for HC-specific promoter in cochlear gene therapy.

We have demonstrated that AAV-PHP.eB can transfect various inner ear cells efficiently, including HCs, sensory epithelial, spiral ganglion, spiral ligaments, stria vascularis, and spiral limbus, but it cannot target HCs specifically.[23] Therefore, in order to achieve specific and efficient HC transgene expression, we packaged the GFP fluorescent reporter gene into the highly efficient AAV-PHP.eB driven by IHC-specific promoter Myo15 and measured the expression and distribution of GFP. Autosomal recessive hearing loss 9 (DFNB9) is caused by a pathogenic mutation of *OTOF* gene.[24] As otoferlin was expressed in IHCs and clinical practice of the gene therapy of DFNB9 is ongoing, we packaged the *OTOF* coding sequence (CDS) into AAV-PHP.eB under the control of Myo15 promoter, aiming to provide a more effective and safer preclinical drug candidate for the therapy of DFNB9.

RESULTS

Myo15 promoter initiates efficient expression of GFP in HCs

To verify the ability of the Myo15 promoter to initiate transcription in HCs, we packaged Myo15 (or CAG) promoter into AAV-PHP.eB to drive the expression of the GFP fluorescence reporter genes. A dose of 1×10^{10} vector genomes (vg) per cochlea was injected into neonatal mice via the round window membrane (RWM) at postnatal days 0–2 (P0–P2). Two weeks after injection, immunofluorescence staining was performed on whole-mount cochlea, and the expression rate of GFP in IHCs and OHCs was determined by the percentage of Myo7a-labeled HCs expressing GFP. As shown in Figure 1, robust GFP expression was observed in both IHCs and OHCs under both promoters, but the Myo15 promoter restricted GFP expression exclusively in the HCs (Figure 1A), while the CAG promoter directed GFP expression not only in the HC region but also in the spiral limbus and spiral ganglion region (Figure 1B). The expression rate of GFP in HCs with the two promoters was further evaluated (Figures 1E and 1F). Under the control of the CAG promoter, GFP was expressed in 97.11% ± 1.51%, 97.57% ± 1.56%, and 93.87% ± 2.96% of the IHCs in the apical, middle, and basal turns, respectively, while under the control of the Myo15 promoter, GFP was expressed in 98.67% ± 1.33%, 98.64% ± 0.99%, and 98.85% ± 1.15% of the IHCs in the apical, middle, and basal turns, respectively. For the OHCs, the Myo15 promoter directed the expression of GFP in 82.80% ± 4.88%, 88.47% ± 3.43%, and 87.07% ± 7.32% in the apical, middle, and basal turns, respectively, compared with 79.94% ± 8.25%, 82.56% ± 6.46%, and 83.83% ± 4.87% under the control of the CAG promoter. There were no statistical differences between the two groups ($p > 0.05$ for all comparisons). These results indicate that the Myo15 promoter can initiate potent and specific expression of transgene in the HCs.

Given that the human cochlea is fully developed while the mouse cochlea matures until postnatal weeks 2–3, we also evaluated the expression efficacy of GFP in adult mice (P30). Two weeks after injection, GFP was expressed in 81.85% ± 9.14%, 98.81% ± 1.19%, and 95.39% ± 2.83% of the IHCs under the control of Myo15 promoter in the apical, middle, and basal turns, respectively; under the control of the CAG promoter, GFP was expressed in 76.18% ± 7.11%, 100% ± 0.00%, and 100% ± 0.00% of the IHCs in the apical, middle, and basal turns, respectively (Figures 1C, 1D, and 1G).

In vestibular HCs, GFP was observed in the utricle HCs, in both newborn and adult mice. Similar to the specificity in cochlear HCs, the Myo15 promoter also drove specific expression in vestibular HCs, while the CAG promoter also directed GFP expression in other cell types (Figure S1).

Systemic injection is a common routine for the therapy of many diseases. Thus we also observed the expression of GFP in adult mouse via tail intravenous injection in a dose of ten times the RWM injection (1×10^{11} vg/mouse, intravenously). The results demonstrated that no GFP was observed in HCs in the cochlea two weeks after injection, neither CAG promoter nor Myo15 promoter (Figure S2). Several factors may account for the negative results, such as inadequate dose of injection, the discrepant transduction efficacies of different AAV serotypes, and the limited number of mice included in this study. Overall, the present results demonstrated that local injection into the inner ear directly can achieve appropriate viral titers for gene therapy instead of systemic administration.[25]

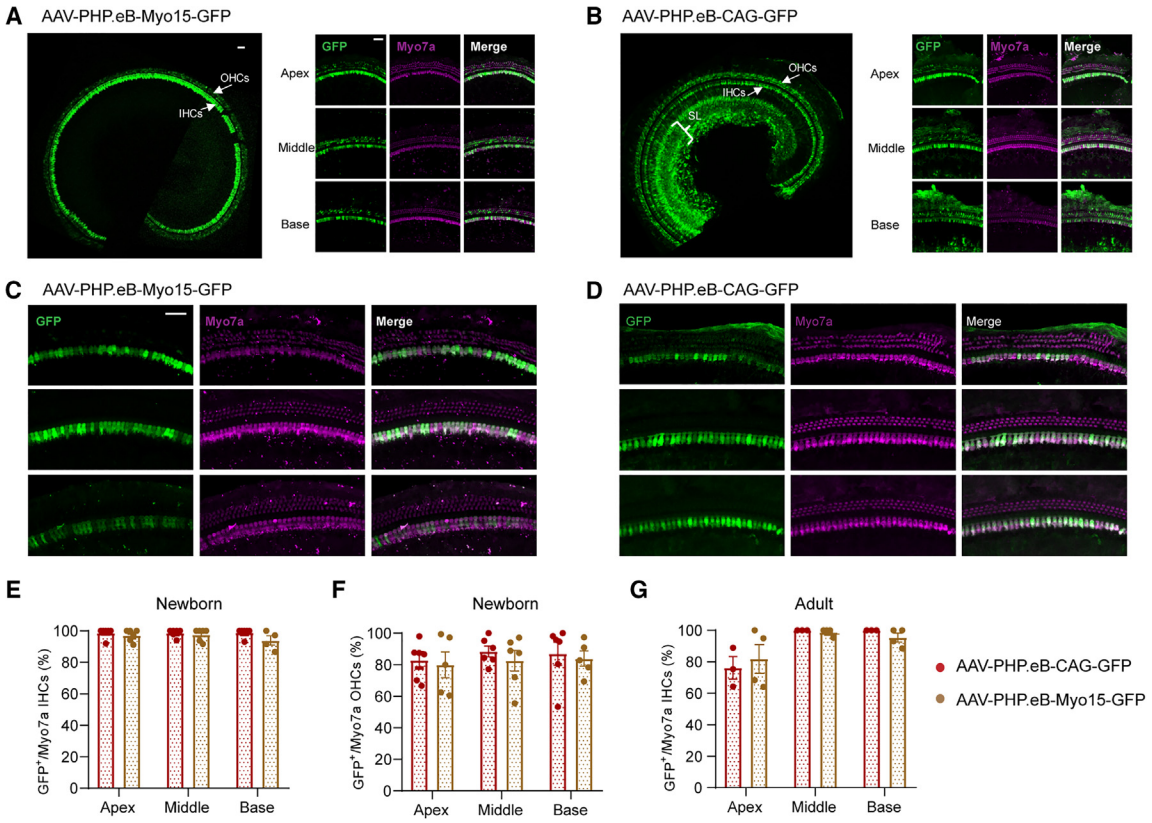

Figure 1. GFP expression in HCs throughout the cochlea under the control of the Myo15 and CAG promoters

(A and B) Representative whole-mount images of the injected ear in mice treated at P0–P2 with PHP.eB-Myo15-GFP (A) and PHP.eB-CAG-GFP (B). Left panel: low-magnification view; right panel: high-magnification views of the apical, middle, and basal turns (B). (C and D) Representative whole-mount images of the injected ear in mice treated on P30 with PHP.eB-Myo15-GFP (C) and PHP.eB-CAG-GFP (D). IHC, inner hair cell; OHC, outer hair cell; SL, spiral limbus. Scale bars: 50 μm. (E and F) Percentages of GFP-positive IHCs (E) and OHCs (F) in the newborn-injected mice. N = 6 mice for each group. (G) Percentages of GFP-positive IHCs adult-injected mice; N = 3 and 4 mice for CAG and Myo15 groups, respectively. Data are displayed as mean ± SEM.

Myo15 promoter initiates specific expression of GFP in HCs

To further confirm the specific expression of the gene of interest under the control of the Myo15 promoter, we observed the distribution of GFP in cochlear cryosections. AAV-PHP.eB packaged with the Myo15 or CAG promoter and the GFP reporter genes were injected as described above. Two weeks after injection, the cochlear cryosections were examined. As shown in Figures 2A and 2B, the CAG promoter directed a broad distribution profile, and the GFP signal was observed in various cochlear cell types, including the lateral wall, the spiral limbus, the tectorial membrane, and the stria vascularis. In contrast, under the control of the Myo15 promoter, the GFP signal was exclusively expressed in the HC region (as identified by phalloidin), and negligible GFP signal was observed in other regions of the cochlea (Figures 2C and 2D).

The cochlear aqueduct may provide a connection between the inner ear and the cerebrospinal fluid (CSF),[26,27] and it is possible that the virus transduces the CNS, which may lead to potential safety issues. Therefore, we examined GFP expression in brain tissues after injection of AAV-PHP.eB under the control of the of Myo15 and CAG promoters. Two weeks after RWM injection at P0–P2, sagittal brain sections were immunostained with anti-GFP primary antibody. As shown in Figures 2E and 2F, the CAG promoter directed obvious GFP expression throughout the brain, and the magnified images confirmed the robust GFP expression in the cerebral cortex, olfactory bulb, hippocampus, and cerebellum. In contrast, AAV-PHP.eB under the control of the Myo15 promoter showed negligible GFP expression in the CNS (Figures 2G and 2H). These results demonstrate that the HC-specific promoter could avoid potential off-target expression of exogenous genes in nontarget tissues.

Additionally, we observed GFP fluorescence in the contralateral non-injected ear in almost all of the AAV-PHP.eB-injected mice. We quantified the expression rate in the contralateral ears and observed expression of GFP in 53.81% ± 5.00% and 64.53% ± 5.53% of the IHCs under the control of the CAG and Myo15 promoters, respectively. In contrast, GFP expression in OHCs was significantly weaker and was counted in 23.08% ± 2.59% and 25.92% ± 6.44% of the OHCs under the control of the CAG and Myo15 promoters, respectively

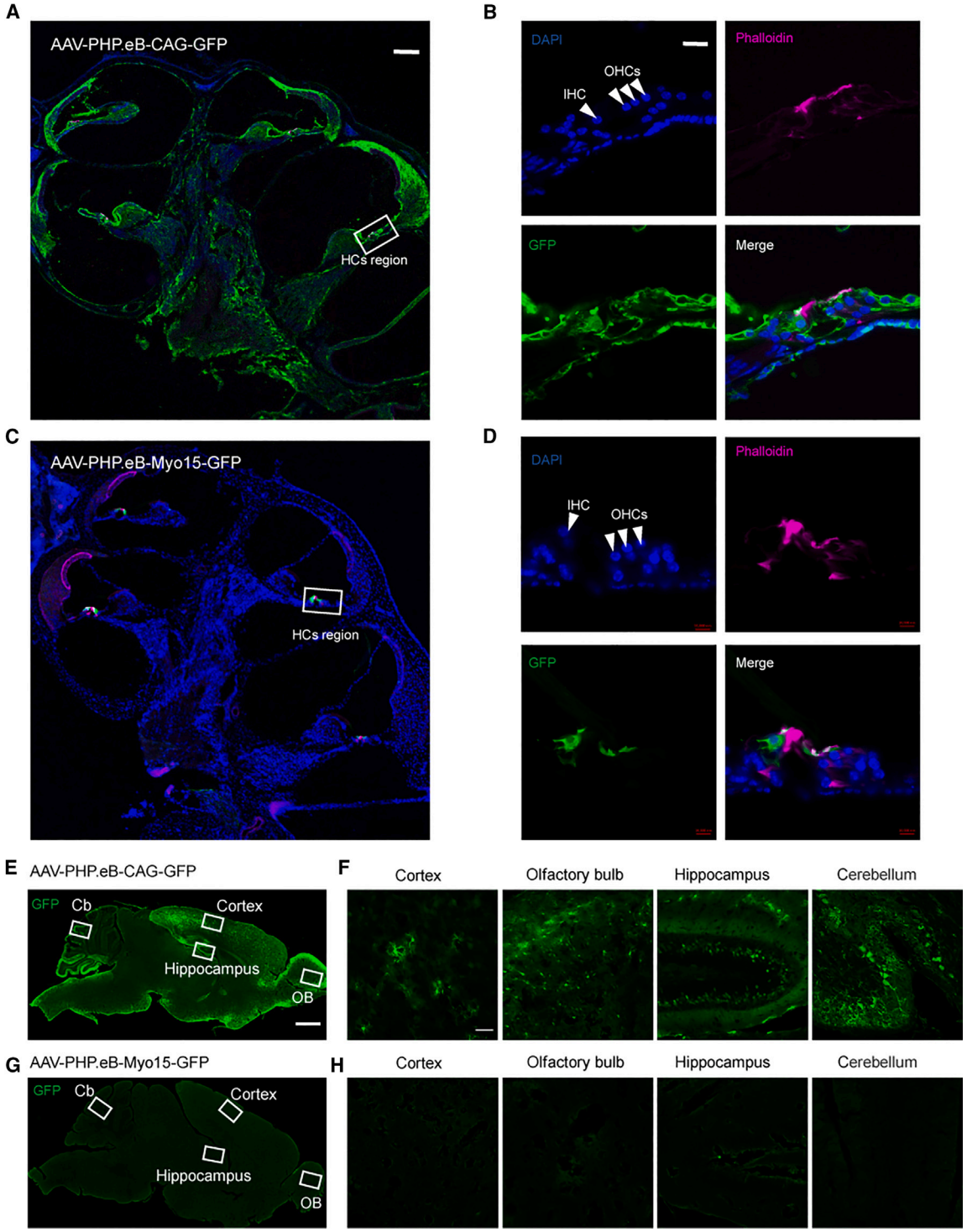

Figure 2. GFP distribution in the cochlea and CNS under the control of the Myo15 and CAG promoters

(A and B) Representative images of frozen sections of the cochlea from a mouse injected with PHP.eB-CAG-GFP. (A) Overall GFP distribution in the cochlea. (B) Enlarged images of the HC region. (C and D) Representative images of frozen sections of the cochlea from a mouse injected with PHP.eB-Myo15-GFP. (C) Overall GFP distribution in

(legend continued on next page)

(Figure S3). Therefore, the AAV-PHP.eB combined with Myo15 promoter can direct transgene expression specifically in bilateral HCs, which might result in bilateral hearing recovery after single unilateral injection.

Hearing in *Otof* $^{-/-}$ mice was rescued by the Myo15-driven *OTOF* CDS

We further tested the transcription ability of the Myo15 promoter as a therapeutic agent in an *Otof* $^{-/-}$ mouse model. The CDS of human *OTOF* was split into two fragments (5′-terminal [*OTOF* NT] and 3′-terminal [*OTOF* CT]), and the fragments were packed into AAV-PHP.eB separately. After co-injection of *OTOF* NT and *OTOF* CT into cochlea, recombination of the two halves of the *OTOF* CDS followed by producing a mature mRNA, and this could be translated into full-length otoferlin *in vivo*. The schematic diagram of the dual-AAV strategy for obtaining full-length otoferlin is shown in Figure S4. To examined the accuracy of the pre-mRNA splicing process of human *OTOF* CDS (NM_001287489.2) in transduced cells, we first detected recombination of N- and C-terminal *OTOF* CDS sequences in DNA level whether the additional donor sequence (SD) and acceptor sequence (SA) were together inserted into split site (between residues 841 and 842). *OTOF* DNA were isolated from the organ of Corti from the treated mice (3–4 weeks after injection) and sequenced. The results showed that the sequence was successfully added into the split site after recombination of full-length *OTOF* CDS (as shown in Figure S5). Then we examined whether the additional SD and SA in full-length *OTOF* were *trans*-spliced in mRNA level, after isolation and reverse transcription of mRNA into cDNA, we found that *trans*-splicing of the split site in full-length *OTOF* completely removed the additional SD and SA by sequencing and alignment analysis (as shown in the Figure S5), indicating that accurate splicing was conducted in the treated mice.

To test the hearing recovery of *Otof* $^{-/-}$ mice after injection of the dual AAV-mediated therapeutic system, PHP.eB-*OTOF* NT driven by the Myo15 (or the CAG promoter) and PHP.eB-*OTOF* CT were mixed in a 1:1 ratio before injection, and 2 μL of the mixture was injected into *Otof* $^{-/-}$ mice at P0–P2 via the RWM. Auditory brainstem response (ABR) recordings in response to click and tone-burst stimuli were performed 3–4 weeks after injection. As shown in Figure 3A, no identifiable ABR waves could be elicited in the untreated *Otof* $^{-/-}$ mice, even at the 90 dB maximum sound pressure level (SPL), while in the dual AAV-treated *Otof* $^{-/-}$ mice (both with the Myo15 and CAG promoters), the characteristic ABR waveforms of the injected ear were elicited. The ABR thresholds for click stimuli were 54.71 ± 3.52 dB and 55.48 ± 2.91 dB for the dual AAV-PHP.eB-Myo15-*OTOF*-treated mice (Myo15 group) and dual AAV-PHP.eB-CAG-*OTOF*-treated mice (CAG group) (Figure 3B). For the tone-burst stimuli, the average thresholds in the Myo15 group were comparable with those of wild-type (WT) mice at 16 and 32 kHz ($p > 0.05$, two-way ANOVA) and approximately 10 dB higher than WT at 4, 8, and 24 kHz ($p = 0.049$, $p = 0.015$, and $p = 0.024$, respectively). Overall, the hearing recovery in the Myo15 group was comparable with that of the CAG group (Figure 3B). Furthermore, hearing in the contralateral ear was also significantly improved in both groups (Figure S6): the average threshold recovered from more than 90 dB (untreated *Otof* $^{-/-}$ mice) to 60–80 dB. In contrast, no recovery was observed in the *Otof* $^{-/-}$ mice receiving either PHP.eB-Myo15-*OTOF* NT or AAV-PHP.eB-*OTOF* CT alone (Figure S7). The amplitude of the ABR wave I, which represents the summed activity of the auditory nerve, was very small in the treated *Otof* $^{-/-}$ mice (both Myo15 and CAG groups) in contrast to WT mice (click stimulus at 90 dB; WT, 6.02 ± 0.42 μV; CAG group, 0.44 ± 0.08 μV; Myo15 group, 0.35 ± 0.13 μV, $p < 0.0001$, one-way ANOVA) (Figure 3C). The latency of the Myo15 group showed no statistical difference compared with that of the WT group (click stimulus at 90 dB; 1.61 ± 0.09 ms vs. WT [1.38 ± 0.05 ms]; $p = 0.056$) (Figure 3C), while the latency of the CAG group (1.63 ± 0.05 ms) was longer than that of WT ($p = 0.015$). Additionally, we observed the long-term hearing recovery and measured the ABR threshold 6 months after the injection of Myo15-driven therapeutic agent. The results showed that the click ABR was 55.00 ± 3.54 dB and had no statistical difference compared with that of 3–4 weeks ($p = 0.97$). For the tone-burst stimuli, the ABR threshold was 76.00 ± 3.67, 59 ± 3.67, 66 ± 3.67, 79 ± 2.45, and 77 ± 2.55 dB for 4, 8, 16, 24, and 32 kHz, respectively. The ABR thresholds at other frequencies had no statistical differences compared with that of 3–4 weeks, except the 24 kHz ($p = 0.003$ for 24 kHz, $p > 0.05$ for other frequencies) (Figure 3D).

We also evaluated the efficacy in *Otof* $^{-/-}$ adult mice (P30). Four weeks after injection, the ABR threshold for click stimuli were recovered to 58.75 ± 4.27 dB for the dual AAV-PHP.eB-Myo15-*OTOF*-injected mice. For the tone-burst stimuli, the average thresholds in the Myo15 group were also rescued significantly (83.75 ± 5.15, 58.75 ± 6.88, 53.75 ± 5.91, 53.75 ± 3.15, and 62.6 ± 6.61 dB for 4, 8, 16, 24, and 32 kHz respectively) (Figure 3E).

We next evaluated the expression of human otoferlin in newborn treated *Otof* $^{-/-}$ mice. Organs of Corti were dissected at P21–P30 and immunostained with a primary antibody against otoferlin. In the dual AAV-PHP.eB-Myo15-*OTOF*-injected ears, we observed otoferlin expression in 72.88% ± 1.93%, 67.68% ± 4.39%, and 52.72% ± 7.2% of the IHCs in the apical, middle, and basal turns, respectively, while in the dual AAV-PHP.eB-CAG-*OTOF*-injected ears, otoferlin was expressed in 59.41% ± 4.14%, 41.40% ± 5.32%, and 30.92% ± 6.95% of the IHCs in the apical, middle, and basal turns of the cochlea, respectively (Figures 3F and 3G). Although the rate of otoferlin expression in the Myo15 group seemed to be higher than that of

the cochlea. (D) Enlarged images of the HC region. Scale bars: 100 μm (A and C) and 10 μm (B and D). (E and F) Representative sagittal brain images from mice injected with PHP.eB-CAG-GFP. (E) Overall GFP distribution in the whole brain. (F) Enlarged images of the cortex, olfactory bulb (OB), hippocampus, and cerebellum (Cb). (G and H) Representative sagittal brain images from a mouse injected with PHP.eB-Myo15-GFP. (G) Overall GFP distribution in the whole brain. (H) Enlarged images of the cortex, olfactory bulb, hippocampus, and cerebellum. Scale bars: 1 mm (E and G) and 100 μm (F and H).

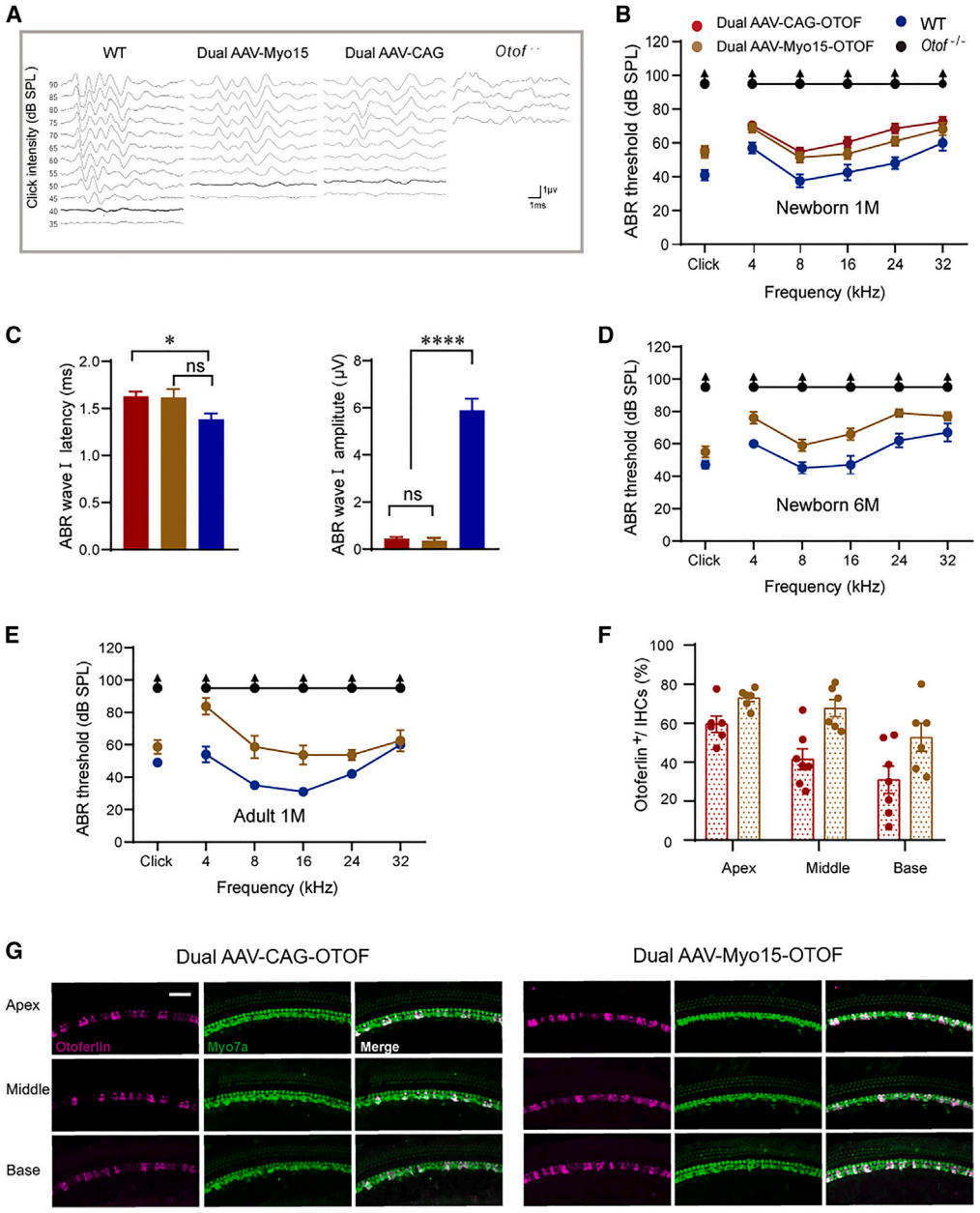

Figure 3. Dual AAV-mediated gene therapy rescues hearing and otoferlin expression in *Otof* $^{-/-}$ mice

(A) Representative ABR traces in response to broadband click sound stimuli recorded at P21–P28 from WT mice, untreated *Otof* $^{-/-}$ mice, and *Otof* $^{-/-}$ mice treated with dual AAV-CAG-*OTOF* and dual AAV-Myo15-*OTOF*. (B) ABR thresholds recorded at P21–P28 from WT mice, untreated *Otof* $^{-/-}$ mice, and dual AAV-CAG-*OTOF*-treated and dual AAV-Myo15-*OTOF*-treated *Otof* $^{-/-}$ mice at different frequencies (N = 10, 8, 21, and 15 for the WT, *Otof* $^{-/-}$, dual AAV-CAG-*OTOF*, and dual AAV-MYO15-*OTOF* groups, respectively). (C) ABR wave I amplitude and latency for 90 dB click stimuli in newborn-injected *Otof* $^{-/-}$ mice compared with WT mice (N = 10, 18, and 9 for the WT, dual AAV-CAG-*OTOF*, and dual AAV-Myo15-*OTOF* groups, respectively). (D) ABR thresholds recorded at 6 months after dual AAV-Myo15-*OTOF* injection (N = 5, 5, and 8 for injected mice, WT, and *Otof* $^{-/-}$ mice, respectively). (E) ABR thresholds recorded at 2 weeks after the dual AAV-Myo15-*OTOF* injection in the adult *Otof* $^{-/-}$ mice (N = 4, 5, and 8 for the injected mice, WT, and *Otof* $^{-/-}$ mice, respectively). (F and G) Otoferlin expression in the newborn-treated *Otof* $^{-/-}$ mice observed at P21–P28. (F) Percentage of otoferlin-labeled IHCs in the injected ear (N = 7 and 6 mice for the CAG and Myo15 groups, respectively); representative images of IHCs immunostained with otoferlin (G). For (B)–(E), red color indicates the dual AAV-CAG-*OTOF*-treated group, brown indicates the dual AAV-Myo15-*OTOF*-treated group, blue indicates the WT group, and black indicates the untreated *Otof* $^{-/-}$ group. Data are displayed as mean ± SEM. ns, not significant; *$p < 0.05$ and ****$p < 0.0001$. Scale bars: 50 μm.

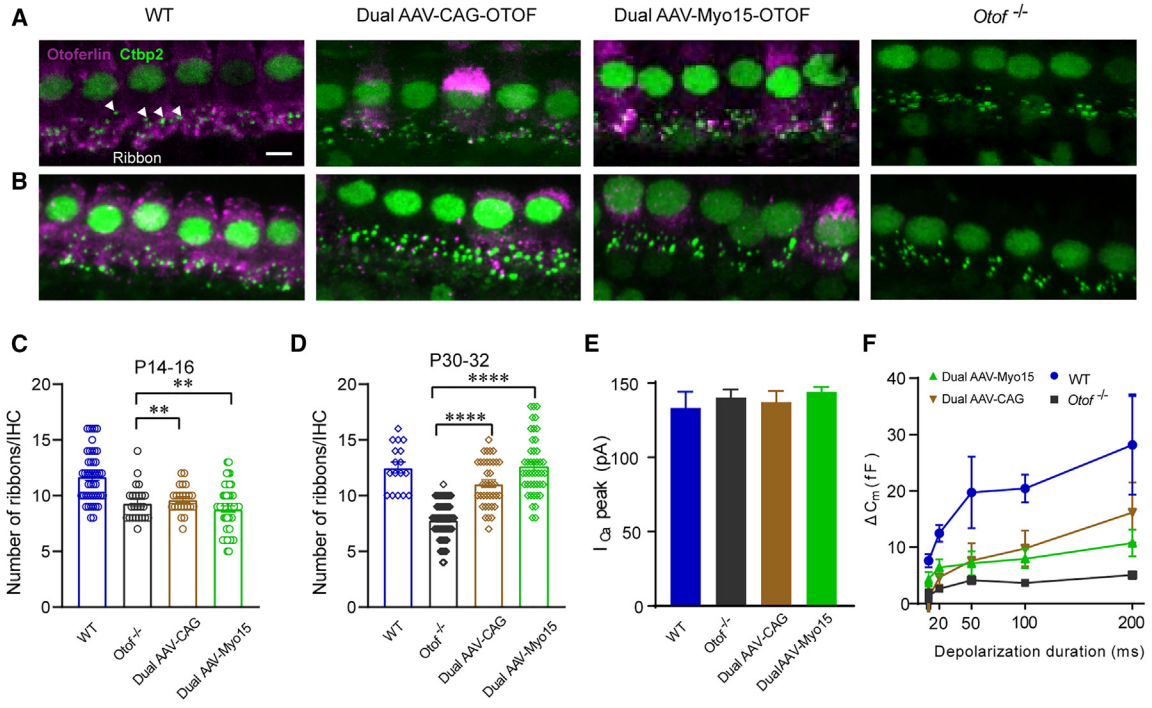

Figure 4. The therapeutic system driven by the Myo15 promoter rescues the synaptic function of IHCs

(A and B) Representative images of synapse ribbons of the apical turn from WT mice, dual AAV-CAG-*OTOF*-treated and dual AAV-Myo15-*OTOF*-treated mice, and untreated *Otof* $^{-/-}$ mice at P14–P16 (A) and P30–P32 (B). Scale bars: 10 μm. The white triangles were used to annotate the ribbons. (C) Number of synaptic ribbons quantified from IHCs in the apical turn at P14–P16. (D) The number of synaptic ribbons quantified from IHCs in the apical turn at P30–P32. (E) Ca^{2+} currents of IHCs at P14–P16. n = 6, 16, 17, and 9 IHCs for WT, untreated *Otof* $^{-/-}$, and dual AAV-Myo15-*OTOF*, and dual AAV-CAG-*OTOF*, respectively. (F) Exocytosis of IHCs evaluated by changes in plasma membrane capacitance increments (ΔC_m). n = 6, 16, 16, and 8 IHCs from the WT, untreated *Otof* $^{-/-}$, dual AAV-Myo15-*OTOF*-treated, and dual AAV-CAG-*OTOF*-treated groups, respectively. Data are displayed as mean ± SEM. For (C)–(E), ns, not significant; ****p < 0.0001.

CAG group, the difference was not statistically significant (p > 0.05 for all comparisons). The otoferlin expression level in this study may not be sufficient to restore hearing in *Otof* $^{-/-}$ mice to the WT level, especially in the middle and basal turns. Therefore, in order to further improve the hearing recovery, measures to improve the recombination efficiency should be taken. All in all, these results indicate that the HC-specific Myo15 promoter can be used to initiate the transcription of a therapeutic gene, it would not hinder the recombination and expression of the two halves of the *OTOF* CDS to generate full-length and functional human otoferlin.

Exocytosis of *Otof* $^{-/-}$ mice was partially rescued by the Myo15-driven *OTOF* CDS

A previous study reported that the number of ribbon synapses formed by *Otof* $^{-/-}$ IHCs was normal at P6, but only 60% of them remained at P15.[7] To evaluate whether the synapse numbers could be rescued in the treated *Otof* $^{-/-}$ IHCs, we counted the number of CtBP2-labeled ribbon synapses two and four weeks after injection, respectively. At P14–P16, the synapse number in the CAG group (9.65 ± 0.26 synapses/IHC, n = 23 from 2 mice) and Myo15 group (8.80 ± 0.28 synapses/IHC, n = 51 from 3 mice) groups was similar to that of untreated mice (9.33 ± 0.32 synapses/IHC, n = 24 from 3 mice) (p > 0.1), and they were significantly less than the WT mice (11.72 ± 0.34 synapses/IHC, n = 46 from 3 mice) (p < 0.005) (Figures 4A and 4C). In contrast, at P30–P32, the synapse numbers in the CAG group (11.08 ± 0.34 synapses/IHC, n = 37 from 3 mice) and Myo15 groups (12.64 ± 0.40 synapses/IHC, n = 44 from 3 mice) were significantly increased, comparable with that of WT mice (12.53 ± 0.50 synapses/IHC, n = 17 from 1 mice) (p > 0.05) (Figures 4B and 4D). In contrast, the number of ribbons per IHC in untreated *Otof* $^{-/-}$ continued to decrease to (7.83 ± 0.21 synapses/IHC, n = 65 from 5 mice) at P30. Subsequently, to investigate whether *OTOF* gene delivery could rescue the exocytosis function of *Otof* $^{-/-}$ mice, we performed cellular electrophysiological recordings. Ca^{2+} currents (I_{Ca}) and plasma membrane capacitance increments (ΔC_m) of the apical turns of the organ of Corti at P14–P18 were measured. Consistent with previous works,[7] the voltage-gated Ca^{2+} current of the treated *Otof* $^{-/-}$ group (CAG group, n = 9 IHCs; Myo15 group, n = 17 IHCs) and the untreated *Otof* $^{-/-}$ group (n = 16 IHCs) (p = 0.6717) were similar to the WT group (n = 6 IHCs) (Figure 4E). After short depolarization pulses (20 ms) eliciting Ca^{2+} influx, IHC plasma membrane capacitance increments (ΔC_m) were recorded as measurements of the rapid exocytosis of the readily releasable pool (RRP) of synaptic vesicles. After 20 ms depolarization pulses, as shown in Figure 4F, ΔC_m was increased from 2.62 ± 0.49 fF

(untreated *Otof*$^{-/-}$ mice) to 6.04 ± 1.48 fF (Myo15 group) ($p = 0.0214$, two-tailed t test), but ΔC_m was smaller than that of WT mice (12.47 ± 1.51 fF) ($p = 0.0347$). In contrast, there was no statistical difference between the untreated and the dual AAV-CAG-*OTOF*-injected ear (4.63 ± 1.42 fF) ($p = 0.1093$). Vesicle replenishment, calculated according to previous formula,[28] failed to be rescued in both treated groups: the mean vesicle supply in the Myo15 group (44.73 ± 33.12 vesicles/s in each active zone) was comparable with that of untreated group (31.11 ± 17.77 vesicles/s in each active zone) ($p = 0.9583$) and was significantly less than WT (167 ± 37.80 vesicles/s in each active zone) ($p < 0.05$). Representative values of ΔC_m of the IHCs in response to 100 ms depolarization are shown in Figure S8.

Last, we evaluated the safety of the therapeutic system. The same dose of therapeutic AAVs was injected into WT 129 mice at P0–P2, and the ABR was assessed 3–4 weeks after injection. There was no difference between the injected ear and noninjected WT mice at all frequencies (Figure S9), suggesting that the therapeutic system was well tolerated. Therefore, the Myo15 promoter can be used as a specific regulator for the gene therapy of hearing loss related to dysfunctions of HCs.

DISCUSSION

In this study, we evaluated the efficiency and specificity of transgene expression under the control of the inner ear sensory cell-specific promoter Myo15. We found that the expression level of the GFP fluorescence reporter gene in HCs was comparable with that of the ubiquitous CAG promoter, while the off-target expression in other cell types of the inner ear and CNS was significantly decreased. In addition, by using the Myo15 promoter, we constructed a novel *OTOF* gene therapeutic system and rescued the expression of otoferlin and exocytosis in IHCs, thereby rescued auditory function in *Otof*$^{-/-}$ mice.

To date, hearing in various mouse models has been successfully rescued by strategy of gene therapy, including *OTOF*, *MYO6*, *STRC*, and *Prestin*.[29–32] However, there is still a long way to go before clinical translation, and safety issues must be fully considered. The engineered AAV-PHP.eB is a novel, potent serotype that was originally used in the CNS[33]; it could effectively transduce HCs in the inner ear, and the hearing loss in several animal models has been rescued by using it as delivery vector; thus AAV-PHP.eB may have great potential in human clinical studies.[30,34] Besides this, AAV-PHP.eB could transduce many other cell types[33,35,36] and thus may lead to off-target expression of transgenes under the control of ubiquitous promoters. Systemic administration of these kinds of therapeutic vectors tends to induce wide-scale transgene expression throughout the body.[9,37,38] A preclinical study revealed degeneration of neurons, liver dysfunction, and coagulation disorders in Wistar Han rats and cynomolgus macaques after intravenous injection of the survival motor neuron 1 (SMN1) therapeutic transgene.[9] A study in marmosets also demonstrated that high-level transgene expression under the control of the ubiquitous CMV promoter induces toxicity and inflammation in neurons in contrast to the neuron-specific promoters (e.g., CaMKII).[10] Local inner ear injection also results in various off-target distributions of the gene of interest, including in the brain and liver.[26,39,40] The cochlea is a relatively isolated organ, so local inner ear injection was adopted instead of systemic administration. The local injection facilitates appropriate viral titers in the inner ear but reduces the viral titers in other organs compared with systematic injection, although it is difficult at present to determine whether Myo15 promoter targets other cell types in humans. HCs are one of the key targets in therapy for hearing loss, as more than half of inherited hearing loss genes are expressed in HCs.[15] HC-specific promoter is of crucial importance to the clinical transformation of cochlear gene therapy. Further clarification of the specificity and safety of Myo15 promoter will be conducted in the future.

Myosins are a superfamily of actin-activated P loop ATPases that regulate fundamental cellular processes such as vesicle trafficking and cytokinesis. Unconventional myosin 15 is indispensable for stereocilia development and maintenance, and it is expressed in the HCs of the organ of Corti and accumulates at the tips of mechanosensory stereocilia.[41] The cellular localization suggests that Myo15 promoter sequence can be used to direct specific transgene expression in HCs. We referred to the sequence of a previous work (US 2021/0388045 A1) and synthesized the Myo15 promoter. We packaged the Myo15 promoter into AAV-PHP.eB, and verified that PHP.eB combined with Myo15 promoter could mediate bilateral transgene expression in HCs specifically after a single unilateral injection while minimizing off-target expression in the nontarget organs and other cell types in the inner ear, including the lateral wall, the spiral limbus, the tectorial membrane, and the stria vascularis.

In rodents, the cochlear aqueduct is patent, and this provides a significant communication passage between the perilymph and the CSF. In humans, however, there is still debate as to whether the cochlear aqueduct is patent.[42,43] Although it appears that most adult human temporal bones are occluded with loose connective tissues, this does not preclude the possibility of viral spread to the CNS. In addition, the internal auditory meatus or modiolus may also provide communication between the CSF and the perilymph.[44,45] Our previous study demonstrated that inner ear injection of AAV-Anc80L65-GFP under the control of ubiquitous CMV promoter in adult mice also resulted in apparent GFP expression in the brain.[40] In this study, under the control of the ubiquitous CAG promoter, injection of 1×10^{10} vg/cochlea via the RWM resulted in apparent GFP expression in several brain regions and in the contralateral ear. In contrast, AAV-PHP.eB with the Myo15 promoter also showed GFP expression of HCs in the contralateral ear but displayed negligible fluorescence signal in the brain regions. Therefore, even though the exogenous therapeutic gene may spread elsewhere, the cell-type-specific promoter can avoid potential off-target expression of the exogenous gene. In addition, as long as the transduction rate is high enough, a single unilateral inner ear injection can result in the recovery of bilateral hearing loss, as previously described.[27]

Pathogenic mutation of *OTOF* causes profound autosomal recessive deafness (DFNB9). Given that the size of the *OTOF* CDS (~6 kb) exceeds the capacity of AAV (~4.7 kb), previous studies

used overloaded AAV systems to deliver full-length *Otof* CDS or packaged truncated *Otof* in a single AAV,[46,47] but these manipulations only achieved partial recovery of hearing or only rescued the electrophysiological function of IHCs. The dual-AAV system that takes advantage of the inherent ability of the AAV genome to form tail-to-head concatemers by end-joining of inverted terminal repeats (ITRs) achieved relatively better therapeutic effects. In this study, *OTOF* NT and *OTOF* CT were packaged into AAV-PHP.eB separately, and co-injection of the dual-AAV therapeutic system resulted in full-length otoferlin expression in the IHCs, in *Otof* $^{-/-}$ mice treated with dual AAV-PHP.eB-Myo15-*OTOF*, otoferlin was detected in approximately 60% of the injected ears. Interestingly, the otoferlin was expressed mainly in IHCs, with almost no expression in OHCs; this phenomenon was also found in previous research,[28] and although the exact mechanism remains obscure, it may be associated with targeted protein degradation or post-transcriptional regulation. Otoferlin is proposed to serve as a Ca^{2+} sensor and plays an important role in exocytosis and vesicle replenishment. Dysfunction of otoferlin leads to abnormal synaptic transmission, so that IHCs cannot transform mechanical acoustic vibration into a neural code.[7,48] In this study, the exocytosis of *Otof* $^{-/-}$ mice was partially rescued by Myo15-driven *OTOF* gene therapy, thereby restoring the hearing function. Besides, the number of ribbons per IHC in injected mice at P30 was significantly increased compared with both treated and untreated *Otof* $^{-/-}$ at P14 and also significantly increased compared with that of untreated *Otof* $^{-/-}$ at P30. This phenomenon was similar to research by Akil et al.,[49] who concluded that the number of ribbons per IHC at P80 (injected at P17) was more than that of noninjected mice at P17. Therefore, the expression of otoferlin may promote the production of ribbons rather than preventing their degeneration in *Otof* $^{-/-}$ mice. Expectedly, the hearing function of *Otof* $^{-/-}$ mice was rescued after injection, and ABR thresholds were improved significantly. The partial recovery of *Otof* $^{-/-}$ mice might be attributed to the limited recombination efficiency of nucleic acid *trans*-splicing. Another recombination strategy is intein-mediated protein *trans*-splicing, the recombination efficiency of which is comparable with that of single AAV injection.[50] Our previous study[29] indicated that hearing of *Otof* $^{-/-}$ mice treated with intein-mediated gene therapy could be restored to WT levels at all frequencies, and the contralateral ear was also restored to 50 dB click stimuli. Therefore, the intein-mediated protein *trans*-splicing strategy together with Myo15 promoter might further improve the efficiency and safety of AAV-mediated gene therapy, but the length of the Myo15 promoter fused with *OTOF* CDS using the intein strategy exceeds 4.7 kb, so optimization of the promoter is worth exploring.

In conclusion, we validated the specific transcription initiation ability of the Myo15 promoter in HCs and rescued the hearing of *Otof* $^{-/-}$ mice using a Myo15 promoter-mediated therapeutic agent. This work not only provides a candidate drug for gene therapy of DFNB9 but also offers a relatively safer reference for gene therapy of other HC-related hearing loss.

MATERIALS AND METHODS

Animals

Otof $^{-/-}$ mice of the 129 strain were established by Biocytogen (Beijing, China), and the details have been described in our previous research.[29] Sanger sequencing analysis was used to confirm the genotype of *Otof* $^{-/-}$ mice. The primers used for genotyping were forward primer: 5′-AGGCTGGATCGAGAG CGTCTTAAGT-3′; reverse primer: 5′-ACCTCACTAGAGTGGTACCCTGAGC-3′. Because of their high fertility, neonatal Institute of Cancer Research (ICR) WT mice were used to evaluate the expression level and profile of the GFP fluorescent reporter. Both male and female mice were used in this study. The animals were housed six in a group in a ventilated and pathogen-free cage with 12-h dark/light cycles with free access to food and water. The use and care of animals complied with the Ethics Committee of Fudan University.

Plasmid construction and AAV production

According to a previous invention (US 2021/0388045 A1), we synthesized the Myo15 promoter, compared its specificity and ability to drive transgene expression with CAG promoter, and developed a therapeutic agent for DFNB9. The elements of the pAAV2-Myo15-GFP plasmid contained the CDS of GFP, AAV2 ITRs, the Myo15 promoter, the woodchuck hepatitis virus post-transcriptional regulatory element (WPRE), and the bovine growth hormone polyadenylation sequence (PolyA). The CAG promoter was used to replace the Myo15 promoter to construct the pAAV2-Myo15-GFP plasmid.

For the therapeutic constructs, the full-length CDS of human *OTOF* (GeneBank: NM_001287489.2) was divided into the 5′-terminal segment (1–2,523 bp) and 3′-terminal segment (2,524–5,991 bp), which were synthesized by Sangon Biotech Co., Ltd. (Shanghai, China). The 5′-terminal construct of pAAV-Myo15-*OTOF* carried the Myo15 promoter, the 5′ fragment of the *OTOF* CDS, and a splice SD site.[51] The Myo15 promoter was replaced with the CAG promoter to obtain the 5′-terminal construct of pAAV-CAG-*OTOF*. The 3′-terminal construct carried a splice SA site, the 3′ fragment of the *OTOF* CDS, an WPRE element, and a PolyA sequence. The key sequence information is provided in the supplemental information.

The expression plasmid of pAAV2-CAG/Myo15-GFP or the 5′-terminal and 3′-terminal constructs of pAAV-Myo15/CAG-*OTOF* were packaged separately into the AAV-PHP.eB capsid. AAV-PHP.eB is an engineered, novel serotype that a heptamer amino acid was inserted into the capsid sequence of AAV9; it transduces the CNS with high efficiency, with a 50-fold increase in multiple brain regions.[33,52] Also, AAV-PHP.eB has been reported to possess high transfection efficiency in multiple cell types in the inner ear.[23] AAV production and purification were performed by PackGene Biotech. The vg titers were determined by qPCR and adjusted to 1×10^{13} vg/mL, and they were stored at −80°C and thawed just before injection.

Viral injection into the cochlea

The animal injection procedure was performed as previously described.[30] Briefly, hypothermia was induced to anesthetize P0–P2 mice until loss of consciousness, and they were maintained on an ice pack during the surgery. The surgery was only performed on the right ear of each animal. A post-auricular incision was made, and the tissue was dissected to expose the RWM. A Nanoliter Microinjection System (WPI) connected to a glass micropipette (WPI, Sarasota, FL) was used to deliver 1 μL AAV-PHP.eB-GFP and 2 μL of the mixed therapeutic agent. The genome copy ratio of the 5′-terminal construct and 3′-terminal construct was 1:1. The speed of the injection was maintained at 5 nL/s. After injection, a 6–0 Vicryl suture was used to close the incision, and the mice were placed on a 37°C heating pad for recovery.

Measurement of ABR

ABR measurements were recorded using the RZ6 Acoustic System (Tucker-Davis Technologies, Alachua, FL) in a sound-proof chamber at 3–4 weeks after injection. Mice were anesthetized using xylazine (10 mg/kg) and ketamine (100 mg/kg) through intraperitoneal injection as previously described.[30] The mouse body temperature was maintained at 37°C with a heating pad during testing. The electrical activity of the brain in response to sound was recorded via electrodes. The recording electrode, the reference electrode, and the ground electrode were inserted into the subcutaneous tissues of the mastoid portion, the vertex, and the rump of the animal, respectively. ABR responses were elicited and subsequently amplified (10,000 times), filtered (0.3–3 kHz passband), and averaged (1,024 responses), and the sound level was decreased from 90 to 20 dB SPL in 5 dB steps. The threshold was determined as the lowest SPL at which a reproducible ABR waveform could be detected. The amplitude of wave I of the ABR was measured from the peak of wave I to the following trough.

Immunohistochemistry and immunofluorescence

For the cochlear tissues, the mice were sacrificed, and their cochleae were rapidly removed. Then the cochleae were irrigated with 4% paraformaldehyde (PFA; E672002-0500; Sangon Biotech) through a hole opened at the apex of cochlea and the round and oval window. They were then immersed in PFA overnight at 4°C and decalcified in 10% EDTA (E671001-0500; Sangon Biotech) until they became soft. For whole-mount sections, the basilar membranes were discreetly isolated. For cochlear cryosections, the cochleae were dehydrated with 15% and 30% sucrose in succession until they sank to the bottom of the solution. The tissues were embedded in OCT medium (G6059; Servicebio), frozen, and cut into 10 μm sections using a freezing microtome (Leica). For the brain tissues, mice were anesthetized with xylazine (10 mg/kg) and ketamine (100 mg/kg) and perfused with 20 mL sterile PBS through the left ventricle of the heart followed by 20 mL PFA. Brains were dissected and fixed overnight in PFA. The tissues were then transferred to sucrose solution, embedded in OCT medium, frozen, and cut into 50 μm serial sagittal sections.

The organ of Corti and the brain tissues were permeabilized with 1% Triton X-100 (A110694; Sangon Biotech) in PBS and blocked in 5% donkey serum (D9663; Sigma-Aldrich) buffer at room temperature for 1 h. Primary antibodies were incubated at 4°C overnight. The tissues were then washed three times with PBS and incubated with secondary antibodies for 2 h at room temperature, followed by washing three times. DAPI (F6057; Sigma-Aldrich) was used to stain the cell nuclei. Cochlear HCs were labeled using Phalloidin-iFluor 555 reagent (1:2,000 dilution; ab176756; Abcam). The following primary antibodies were used: chicken IgY anti-GFP (1:500 dilution; ab13970; Abcam), mouse IgG1 anti-otoferlin (1:200 dilution; ab53233; Abcam), rabbit IgG anti-otoferlin (1:200 dilution; PA5-52935; Invitrogen), and mouse IgG1 anti-CtBP2 (1:200 dilution; 612044; BD BioSciences). The following secondary antibodies were used: Alexa Fluor 555-conjugated anti-mouse IgG1 (1:500 dilution; A21127; Invitrogen), Alexa Fluor 647-conjugated anti-rabbit (1:500 dilution; A31573; Invitrogen), and Alexa Fluor 488-conjugated anti-chicken IgY (1:500 dilution; A11039; Invitrogen). A Leica TCS SP8 laser scanning confocal microscope was used to collect the fluorescent z stack images (cochlear section 10/63× objective; cochlear whole-mount 40× objective; brain sections 20× objective), and an Olympus VS120 was used to collect the images of whole-brain sagittal sections. The maximum intensity projections of optical confocal sections are showed in the images. The expression efficacy of otoferlin was calculated by the percentage of IHCs expressing otoferlin. Ribbon counts were established per IHC in the apical turn from the WT mice, treated *Otof* $^{-/-}$ mice (otoferlin-positive IHCs), or untreated *Otof* $^{-/-}$ mice.

DNA isolation, mRNA isolation, RT-PCR, and sequencing

Genomic DNA was extracted from the organ of Corti using QuickExtract DNA Extraction Solution (#QE09050; Epicentre) following the manufacturer's instructions. Three groups were included: WT mice, untreated *Otof* $^{-/-}$ mice, and newborn-injected *Otof* $^{-/-}$ mice (3 weeks after injection). The target sites that spanning the split site and inserts (SD and SA) were PCR amplified. The following primers were used: forward primer: 5′-gagggagctggaaaacatgg-3′; reverse primer: 5′-agagcgtcttgaccttggc-3′. Total mRNA was isolated from organ of Corti using RNAiso Plus (9109; TaKaRa) according to manufacturer's instructions. Then the *OTOF* cDNA fragments spanning the split-site were reversed transcribed (RR037A; TaKaRa), and amplified (RR820A' TaKaRa). The following primers were used: forward primers 5′-tggcggacgagccccagcaca-3′; reverse primers 5′-tgtgctggggctcgtccgcca-3′. The PCR products were purified with a Gel DNA Extraction Kit (#DC301; Vazyme) and subsequently sequenced.

Patch clamping for electrophysiology

To determine if exocytosis of synaptic vesicles was rescued, we performed whole-cell patch-clamp recordings in IHCs of the sensory epithelium from WT, dual AAV-treated *Otof*$^{-/-}$ mice, and untreated *Otof*$^{-/-}$ mice at P14–P18. I_{Ca} and ΔC_m were measured at room temperature as previously described.[30] Briefly, the apical turns of the organ of Corti were isolated and bathed in an oxygenated extracellular solution containing 5.8 mM KCl, 125 mM NaCl, 0.9 mM $MgCl_2$, 5 mM $CaCl_2$, 5.6 mM D-glucose, 10 mM HEPES, 0.7 mM

$NaH_2PO_4 \cdot H_2O$, and 2 mM Na-pyruvate (~300 mOsm, pH 7.40). An upright microscope (Olympus) with a 60× water immersion objective was used to visualize the tissues, and an EPC10 amplifier (HEKA Electronics, Lambrecht Pfalz, Germany) driven by Patchmaster software was used to perform the patch-clamp recordings. The recording pipettes (typically 5–6 MΩ resistance) were pulled from borosilicate glass capillaries (Sutter), coated with dental wax, and filled with 135 mM Cs-methane sulfonate, 10 mM CsCl, 10 mM TEA-Cl, 2 mM EGTA, 10 mM HEPES, 3 mM Mg-ATP, and 0.5 mM Na-GTP (~290 mOsm, pH 7.20). All chemical reagents were purchased from Sigma-Aldrich. The liquid junction potential was corrected offline for all recorded potentials. I_{Ca} was measured using a voltage ramp from a holding potential of −90 to +70 mV in 0.3 s increments, and the resulting current was recorded. Whole-cell C_m was measured using the lock-in feature and the "sine + DC" method. Sine waves of 1 kHz and 50 mV (peak to peak) were superposed onto the holding potential before and after a step depolarization (0 mV, 500 ms), and C_m was determined by the resulting current responses. Exocytosis of IHCs was assessed by the net increase of capacitance before and after stimulation (ΔC_m), the estimated vesicle replenishment rate was calculated as previously described.[28]

Statistical analysis

All statistical analyses were performed using GraphPad Prism version 8.0. Student's t test was used to analyze the differences between two groups. Comparisons of data with more than two groups were analyzed using one-way ANOVA, followed by Tukey's multiple-comparisons test for selected pairs of means. "N" was defined as the number of mouse, while "n" as the number of IHC in this study. Data are presented as mean ± SEM, as noted in the text and figure legends. The p values < 0.05 were considered to indicate statistical significance.

DATA AND CODE AVAILABILITY

All data and materials associated with this study are presented in the paper or the supplemental information.

SUPPLEMENTAL INFORMATION

Supplemental information can be found online at https://doi.org/10.1016/j.omtn.2024.102135.

ACKNOWLEDGMENTS

We thank Shanghai Medical College and Zhongshan Hospital Immunotherapy Translational Research Center for suggestions and assistance in the partial experiments. This work was supported by the National Natural Science Foundation of China (grants 82225014, 82171148, and 82192860), the National Key R&D Program of China (grant 2020YFA0908201 and 2023YFC2508000), the Clinical Research Plan of SHDC (grant SHDC2020CR4083), the Science and Technology Commission of Shanghai (grant 21S11905100), the Special Project for Clinical Research in Health Industry of Shanghai Municipal Health Commission (grant 20224Z0003), the Shuguang Program of Shanghai Education Development Foundation and the Shanghai Municipal Education Commission (grant 20SG08), the Natural Science Key Project of Scientific Research Innovation Program of Shanghai Education Commission (grant 2023ZKZD12), and the Special Research of Prevention and Rehabilitation in Hearing and Language Disabilities belongs to China Disabled Persons' Federation (and 2022CDPFHS-03).

AUTHOR CONTRIBUTIONS

H.W., M.X., L.Z., and Jun Lv performed the experiments. J.Z. performed electrophysiology. Y.S., H.L., and W.W. developed and supervised designed the project. H.W., M.X., and H.T. analyzed the data for the project and wrote the manuscript. Y.S., H.L., W.W., G.L., Jiangping Liu, Y.C., D.W., H.T., and S.H. reviewed and revised the manuscript. All authors read and approved the final manuscript.

DECLARATION OF INTERESTS

All authors declare no competing interests.

REFERENCES

1. GBD 2017 Disease and Injury Incidence and Prevalence Collaborators (2018). Global, regional, and national incidence, prevalence, and years lived with disability for 354 diseases and injuries for 195 countries and territories, 1990-2017: a systematic analysis for the Global Burden of Disease Study 2017. Lancet *392*, 1789–1858.

2. Morton, C.C., and Nance, W.E. (2006). Newborn hearing screening–a silent revolution. N. Engl. J. Med. *354*, 2151–2164.

3. Wesarg, T., Richter, N., Hessel, H., Günther, S., Arndt, S., Aschendorff, A., Laszig, R., and Hassepass, F. (2015). Binaural integration of periodically alternating speech following cochlear implantation in subjects with profound sensorineural unilateral hearing loss. Audiol. Neurootol. *20* (*Suppl 1*), 73–78.

4. Jiam, N.T., Caldwell, M.T., and Limb, C.J. (2017). What Does Music Sound Like for a Cochlear Implant User? Otol. Neurotol. *38*, e240–e247.

5. Korver, A.M.H., Smith, R.J.H., Van Camp, G., Schleiss, M.R., Bitner-Glindzicz, M.A.K., Lustig, L.R., Usami, S.I., and Boudewyns, A.N. (2017). Congenital hearing loss. Nat. Rev. Dis. Primers *3*, 16094.

6. Guan, Y., Du, H.B., Yang, Z., Wang, Y.Z., Ren, R., Liu, W.W., Zhang, C., Zhang, J.H., An, W.T., Li, N.N., et al. (2023). Deafness-Associated ADGRV1 Mutation Impairs USH2A Stability through Improper Phosphorylation of WHRN and WDSUB1 Recruitment. Adv. Sci. *10*, e2205993.

7. Roux, I., Safieddine, S., Nouvian, R., Grati, M., Simmler, M.C., Bahloul, A., Perfettini, I., Le Gall, M., Rostaing, P., Hamard, G., et al. (2006). Otoferlin, defective in a human deafness form, is essential for exocytosis at the auditory ribbon synapse. Cell *127*, 277–289.

8. Ling, Q., Herstine, J.A., Bradbury, A., and Gray, S.J. (2023). AAV-based in vivo gene therapy for neurological disorders. Nat. Rev. Drug Discov. *22*, 789–806.

9. Palazzi, X., Pardo, I.D., Sirivelu, M.P., Newman, L., Kumpf, S.W., Qian, J., Franks, T., Lopes, S., Liu, J., Monarski, L., et al. (2022). Biodistribution and Tolerability of AAV-PHP.B-CBh-SMN1 in Wistar Han Rats and Cynomolgus Macaques Reveal Different Toxicologic Profiles. Hum. Gene Ther. *33*, 175–187.

10. Watakabe, A., Ohtsuka, M., Kinoshita, M., Takaji, M., Isa, K., Mizukami, H., Ozawa, K., Isa, T., and Yamamori, T. (2015). Comparative analyses of adeno-associated viral vector serotypes 1, 2, 5, 8 and 9 in marmoset, mouse and macaque cerebral cortex. Neurosci. Res. *93*, 144–157.

11. Driver, E.C., and Kelley, M.W. (2020). Development of the cochlea. Development *147*, dev162263.

12. LeMasurier, M., and Gillespie, P.G. (2005). Hair-cell mechanotransduction and cochlear amplification. Neuron *48*, 403–415.

13. Zhang, Y., Fang, Q., Wang, H., Qi, J., Sun, S., Liao, M., Wu, Y., Hu, Y., Jiang, P., Cheng, C., et al. (2023). Increased mitophagy protects cochlear hair cells from aminoglycoside-induced damage. Autophagy *19*, 75–91.

14. He, Z.H., Li, M., Fang, Q.J., Liao, F.L., Zou, S.Y., Wu, X., Sun, H.Y., Zhao, X.Y., Hu, Y.J., Xu, X.X., et al. (2021). FOXG1 promotes aging inner ear hair cell survival through activation of the autophagy pathway. Autophagy *17*, 4341–4362.
15. Ahmed, H., Shubina-Oleinik, O., and Holt, J.R. (2017). Emerging Gene Therapies for Genetic Hearing Loss. J. Assoc. Res. Otolaryngol. *18*, 649–670.
16. Del Castillo, I., Morín, M., Domínguez-Ruiz, M., and Moreno-Pelayo, M.A. (2022). Genetic etiology of non-syndromic hearing loss in Europe. Hum. Genet. *141*, 683–696.
17. Jiang, L., Wang, D., He, Y., and Shu, Y. (2023). Advances in gene therapy hold promise for treating hereditary hearing loss. Mol. Ther. *31*, 934–950.
18. Chellappa, R., Li, S., Pauley, S., Jahan, I., Jin, K., and Xiang, M. (2008). Barhl1 regulatory sequences required for cell-specific gene expression and autoregulation in the inner ear and central nervous system. Mol. Cell Biol. *28*, 1905–1914.
19. Sage, C., Huang, M., Vollrath, M.A., Brown, M.C., Hinds, P.W., Corey, D.P., Vetter, D.E., and Chen, Z.Y. (2006). Essential role of retinoblastoma protein in mammalian hair cell development and hearing. Proc. Natl. Acad. Sci. USA *103*, 7345–7350.
20. Boëda, B., Weil, D., and Petit, C. (2001). A specific promoter of the sensory cells of the inner ear defined by transgenesis. Hum. Mol. Genet. *10*, 1581–1589.
21. Liu, Y., Okada, T., Nomoto, T., Ke, X., Kume, A., Ozawa, K., and Xiao, S. (2007). Promoter effects of adeno-associated viral vector for transgene expression in the cochlea in vivo. Exp. Mol. Med. *39*, 170–175.
22. Caberlotto, E., Michel, V., Foucher, I., Bahloul, A., Goodyear, R.J., Pepermans, E., Michalski, N., Perfettini, I., Alegria-Prévot, O., Chardenoux, S., et al. (2011). Usher type 1G protein sans is a critical component of the tip-link complex, a structure controlling actin polymerization in stereocilia. Proc. Natl. Acad. Sci. USA *108*, 5825–5830.
23. Hu, X., Wang, J., Yao, X., Xiao, Q., Xue, Y., Wang, S., Shi, L., Shu, Y., Li, H., and Yang, H. (2019). Screened AAV variants permit efficient transduction access to supporting cells and hair cells. Cell Discov. *5*, 49.
24. Yasunaga, S., Grati, M., Cohen-Salmon, M., El-Amraoui, A., Mustapha, M., Salem, N., El-Zir, E., Loiselet, J., and Petit, C. (1999). A mutation in OTOF, encoding otoferlin, a FER-1-like protein, causes DFNB9, a nonsyndromic form of deafness. Nat. Genet. *21*, 363–369.
25. Omichi, R., Shibata, S.B., Morton, C.C., and Smith, R.J.H. (2019). Gene therapy for hearing loss. Hum. Mol. Genet. *28*, R65–R79.
26. Landegger, L.D., Pan, B., Askew, C., Wassmer, S.J., Gluck, S.D., Galvin, A., Taylor, R., Forge, A., Stankovic, K.M., Holt, J.R., and Vandenberghe, L.H. (2017). A synthetic AAV vector enables safe and efficient gene transfer to the mammalian inner ear. Nat. Biotechnol. *35*, 280–284.
27. Nist-Lund, C.A., Pan, B., Patterson, A., Asai, Y., Chen, T., Zhou, W., Zhu, H., Romero, S., Resnik, J., Polley, D.B., et al. (2019). Improved TMC1 gene therapy restores hearing and balance in mice with genetic inner ear disorders. Nat. Commun. *10*, 236.
28. Al-Moyed, H., Cepeda, A.P., Jung, S., Moser, T., Kügler, S., and Reisinger, E. (2019). A dual-AAV approach restores fast exocytosis and partially rescues auditory function in deaf otoferlin knock-out mice. EMBO Mol. Med. *11*, e9396.
29. Tang, H., Wang, H., Wang, S., Hu, S.W., Lv, J., Xun, M., Gao, K., Wang, F., Chen, Y., Wang, D., et al. (2023). Hearing of Otof-deficient mice restored by trans-splicing of N- and C-terminal otoferlin. Hum. Genet. *142*, 289–304.
30. Xue, Y., Hu, X., Wang, D., Li, D., Li, Y., Wang, F., Huang, M., Gu, X., Xu, Z., Zhou, J., et al. (2022). Gene editing in a Myo6 semi-dominant mouse model rescues auditory function. Mol. Ther. *30*, 105–118.
31. Shubina-Oleinik, O., Nist-Lund, C., French, C., Rockowitz, S., Shearer, A.E., and Holt, J.R. (2021). Dual-vector gene therapy restores cochlear amplification and auditory sensitivity in a mouse model of DFNB16 hearing loss. Sci. Adv. *7*, eabi7629.
32. Tao, Y., Liu, X., Yang, L., Chu, C., Tan, F., Yu, Z., Ke, J., Li, X., Zheng, X., Zhao, X., et al. (2022). AAV-ie-K558R mediated cochlear gene therapy and hair cell regeneration. Signal Transduct. Target. Ther. *7*, 109.
33. Chan, K.Y., Jang, M.J., Yoo, B.B., Greenbaum, A., Ravi, N., Wu, W.L., Sánchez-Guardado, L., Lois, C., Mazmanian, S.K., Deverman, B.E., and Gradinaru, V. (2017). Engineered AAVs for efficient noninvasive gene delivery to the central and peripheral nervous systems. Nat. Neurosci. *20*, 1172–1179.
34. Zheng, Z., Li, G., Cui, C., Wang, F., Wang, X., Xu, Z., Guo, H., Chen, Y., Tang, H., Wang, D., et al. (2022). Preventing autosomal-dominant hearing loss in Bth mice with CRISPR/CasRx-based RNA editing. Signal Transduct. Target. Ther. *7*, 79.
35. Palfi, A., Chadderton, N., Millington-Ward, S., Post, I., Humphries, P., Kenna, P.F., and Farrar, G.J. (2022). AAV-PHP.eB transduces both the inner and outer retina with high efficacy in mice. Mol. Ther. Methods Clin. Dev. *25*, 236–249.
36. Mathiesen, S.N., Lock, J.L., Schoderboeck, L., Abraham, W.C., and Hughes, S.M. (2020). CNS Transduction Benefits of AAV-PHP.eB over AAV9 Are Dependent on Administration Route and Mouse Strain. Mol. Ther. Methods Clin. Dev. *19*, 447–458.
37. Zincarelli, C., Soltys, S., Rengo, G., and Rabinowitz, J.E. (2008). Analysis of AAV serotypes 1-9 mediated gene expression and tropism in mice after systemic injection. Mol. Ther. *16*, 1073–1080.
38. Jackson, K.L., Dayton, R.D., Deverman, B.E., and Klein, R.L. (2016). Better Targeting, Better Efficiency for Wide-Scale Neuronal Transduction with the Synapsin Promoter and AAV-PHP.B. Front. Mol. Neurosci. *9*, 116.
39. Marcovich, I., Baer, N.K., Shubina-Oleinik, O., Eclov, R., Beard, C.W., and Holt, J.R. (2022). Optimized AAV Vectors for TMC1 Gene Therapy in a Humanized Mouse Model of DFNB7/11. Biomolecules *12*, 914.
40. Zhao, Y., Zhang, L., Wang, D., Chen, B., and Shu, Y. (2022). Approaches and Vectors for Efficient Cochlear Gene Transfer in Adult Mouse Models. Biomolecules *13*, 38.
41. Rich, S.K., Baskar, R., and Terman, J.R. (2021). Propagation of F-actin disassembly via Myosin15-Mical interactions. Sci. Adv. *7*, eabg0147.
42. Bachor, E., Byahatti, S., and Karmody, C.S. (1999). New aspects in the histopathology of the cochlear aqueduct in children. Am. J. Otol. *20*, 612–620.
43. Włodyka, J. (1978). Studies on cochlear aqueduct patency. Ann. Otol. Rhinol. Laryngol. *87* (1 Pt 1), 22–28.
44. Tinling, S.P., and Chole, R.A. (1994). Apical cochlear nerve exposed to perilymph in the gerbil and rat. Hear. Res. *73*, 203–208.
45. Stöver, T., Yagi, M., and Raphael, Y. (2000). Transduction of the contralateral ear after adenovirus-mediated cochlear gene transfer. Gene Ther. *7*, 377–383.
46. Rankovic, V., Vogl, C., Dörje, N.M., Bahader, I., Duque-Afonso, C.J., Thirumalai, A., Weber, T., Kusch, K., Strenzke, N., and Moser, T. (2020). Overloaded Adeno-Associated Virus as a Novel Gene Therapeutic Tool for Otoferlin-Related Deafness. Front. Mol. Neurosci. *13*, 600051.
47. Tertrais, M., Bouleau, Y., Emptoz, A., Belleudy, S., Sutton, R.B., Petit, C., Safieddine, S., and Dulon, D. (2019). Viral Transfer of Mini-Otoferlins Partially Restores the Fast Component of Exocytosis and Uncovers Ultrafast Endocytosis in Auditory Hair Cells of Otoferlin Knock-Out Mice. J. Neurosci. *39*, 3394–3411.
48. Johnson, C.P., and Chapman, E.R. (2010). Otoferlin is a calcium sensor that directly regulates SNARE-mediated membrane fusion. J. Cell Biol. *191*, 187–197.
49. Akil, O., Dyka, F., Calvet, C., Emptoz, A., Lahlou, G., Nouaille, S., Boutet de Monvel, J., Hardelin, J.P., Hauswirth, W.W., Avan, P., et al. (2019). Dual AAV-mediated gene therapy restores hearing in a DFNB9 mouse model. Proc. Natl. Acad. Sci. USA *116*, 4496–4501.
50. Tornabene, P., Trapani, I., Minopoli, R., Centrulo, M., Lupo, M., de Simone, S., Tiberi, P., Dell'Aquila, F., Marrocco, E., Iodice, C., et al. (2019). Intein-mediated protein trans-splicing expands adeno-associated virus transfer capacity in the retina. Sci. Transl. Med. *11*, eaav4523.
51. Trapani, I., Colella, P., Sommella, A., Iodice, C., Cesi, G., de Simone, S., Marrocco, E., Rossi, S., Giunti, M., Palfi, A., et al. (2014). Effective delivery of large genes to the retina by dual AAV vectors. EMBO Mol. Med. *6*, 194–211.
52. Deverman, B.E., Pravdo, P.L., Simpson, B.P., Kumar, S.R., Chan, K.Y., Banerjee, A., Wu, W.L., Yang, B., Huber, N., Pasca, S.P., and Gradinaru, V. (2016). Cre-dependent selection yields AAV variants for widespread gene transfer to the adult brain. Nat. Biotechnol. *34*, 204–209.